

Interference Exploitation-based Hybrid Precoding with Robustness Against Phase Errors

Ganapati Hegde, *Student Member, IEEE*, Christos Masouros, *Senior Member, IEEE*, Marius Pesavento, *Member, IEEE*,

Abstract—

Hybrid analog-digital precoding significantly reduces the hardware costs in massive MIMO transceivers when compared to fully-digital precoding at the expense of increased transmit power. In order to mitigate the above shortfall we use the concept of constructive interference-based precoding, which has been shown to offer significant transmit power savings when compared with the conventional interference-suppression-based precoding in fully-digital multiuser MIMO systems. Moreover, in order to circumvent the potential quality-of-service degradation at the users due to the hardware impairments in the transmitters, we judiciously incorporate robustness against such vulnerabilities in the precoder design. Since the undertaken constructive interference-based robust hybrid precoding problem is nonconvex with infinite constraints and thus difficult to solve optimally, we decompose the problem into two subtasks, namely, analog precoding and digital precoding. In this paper we propose an algorithm to compute the optimal constructive interference-based robust digital precoders. Furthermore, we devise a scheme to facilitate the implementation of the proposed algorithm in low-complexity and distributed manner. We also discuss block-level analog precoding techniques. Simulation results demonstrate the superiority of the proposed algorithm and its implementation scheme over the state-of-the-art methods.

I. INTRODUCTION

Massive multiple-input multiple-output (MIMO) system, in which the base stations (BSs) are equipped with hundreds of antennas, is one of the key pillars of the upcoming 5G mobile networks to enable immensely high spectral efficiency [1, 2]. Similar as in the conventional MIMO systems - which comprises only a few antennas (typically less than ten), the degrees of freedom resulting from the large antenna array can be used to form narrow transmit beams using precoding in a massive MIMO downlink system. Even though the precoding techniques that were developed over the decades for the MIMO systems [3, 4] are theoretically extendable to the massive MIMO systems, they are often practically unsuitable because the conventional precoding techniques are employed in the digital baseband domain and they require a dedicated radio-frequency (RF) chain for each antenna element. However the cost and power footprints of the RF chains pose

Ganapati Hegde and Marius Pesavento are with the Communication Systems Group, Technische Universität Darmstadt, Darmstadt 64283, Germany. (e-mail: hegde@nt.tu-darmstadt.de; pesavento@nt.tu-darmstadt.de). Christos Masouros is with the Department of Electronic & Electrical Engineering, University College London, London WC1E7JE, U.K. (e-mail: c.masouros@ucl.ac.uk)

This work has been submitted to the IEEE for possible publication. Copyright may be transferred without notice, after which this version may no longer be accessible.

a significant obstacle in practical implementations when the number of antennas grows large [5]. Therefore devising novel precoding schemes while keeping the hardware costs and power efficiency in mind to make them compatible for massive MIMO systems is inevitable.

One of the solutions to reduce the hardware costs in a massive MIMO system proposed in the literature is hybrid analog-digital precoding [6–9], which requires significantly fewer RF chains compared to the antenna elements. In this system, the RF chains are connected to the antenna elements through analog phase shifters (PSs). The hybrid precoding is performed in two stages: digital precoding in the baseband domain and analog precoding using PSs in the RF domain. In a downlink system, the transmit symbols are first applied with digital precoders (DPs) and the resulting signals are fed to RF chains. The output of the RF chains are processed using analog precoders (APs) and subsequently fed to the antenna elements as shown in Fig. 1.

Hybrid precoding can significantly reduce the hardware costs at the expense of reduced spectral efficiency or increased transmit power to satisfy a certain quality-of-service (QoS) requirement, when compared to the fully-digital precoding [10–12]. Therefore, schemes to improve the energy efficiency are even more desirable in a hybrid precoding-based networks than in the traditional networks. The constructive interference-(CI) based precoding, in which the interference power is exploited to improve the useful signal power at the users, has shown to offer significant transmit power saving in a fully-digital multiuser downlink system [13–16] when compared to the conventional interference-suppression or cancellation-based precoding schemes [4, 17]. Therefore it is judicious to extend the CI-based precoding to hybrid precoding architec-

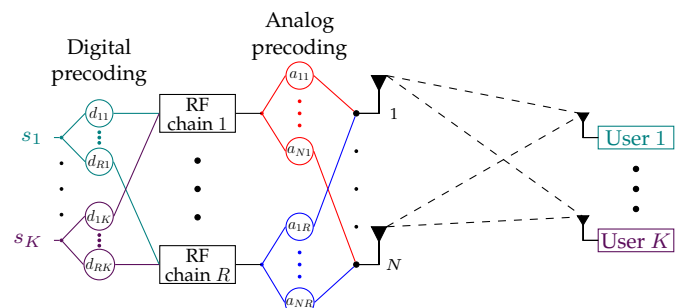


Fig. 1: Schematic diagram of hybrid analog-digital precoding system architecture.

tures in order to reduce the required transmit power. Some initial results in this direction are found in [18].

Some of the envisioned use-cases of 5G networks, such as vehicle-to-x communication and industrial WLAN, require ultra-reliable communication [19]. Therefore, it is crucial to foster the precoders with robustness against interference, imperfect channel knowledge, hardware impairments, etc., in order to guarantee a certain QoS in all circumstances. In [20] the authors develop a method to design the interference-suppression-based hybrid precoders (HPs) with robustness against multiple access interference, inter-symbol interference, and errors in the PSs. In [13, 21] the authors extend the CI-based precoding to design precoders that are robust against imperfect channel knowledge in a fully-digital precoding architecture. The CI-based precoding, in which the precoders are majorly determined by the phase values of transmit symbols and channel elements [13], can be highly sensitive to the phase errors in PSs. However, to the best of our knowledge, the problem of designing the CI-based HPs with robustness against phase errors in the PSs - which is the main focus of this paper - is not considered in the literature.

In this paper we consider symbol-level precoding¹ in a multiuser massive MIMO downlink system. Our goal is to design CI-based HPs that require minimum transmit power to guarantee a certain QoS to the users in the presence of phase errors in the PSs. The resulting optimization problem is nonconvex and contains an infinite constraints, and thus difficult to solve optimally. To deal with the nonconvexity, we propose a method to solve the joint analog and digital precoding problem suboptimally, where we decompose the problem into two sequential subtasks, namely, analog precoding and digital precoding. First, we design the DPs under the premise that the APs are fixed. Subsequently, we discuss various schemes to obtain the APs. The main contributions of this paper are summarized below:

- The CI-based robust digital precoding problem is formulated as a semi-infinite program. An iterative algorithm is proposed to solve the formulated problem. Closed-form expressions are derived to obtain the error matrices, which are required to update the constraint sets in each iteration. The convergence of the algorithm to the optimal point is proven.
- A descent-direction-based iterative scheme is devised to facilitate the distributed implementation of the proposed algorithm on parallel hardware architecture. Closed-form expressions are derived for the update direction and step-size - which are required in a descent direction method [22].
- To relax the strict latency requirements on the APs update, we propose block-level analog precoding.

The paper is organized as follows. In Section II we present the system model. The optimization problem is formulated in Section III. In Section IV we propose an algorithm to design the optimal robust DPs. We develop an iterative scheme to efficiently implement the proposed algorithm in Section V. We present the block-level analog precoding methods in Sec-

tion VI. The numerical results are presented in Section VII. Finally, Section VIII concludes the paper.

Notation: Bold lower-case letters (e.g., \mathbf{a}) denote vectors and bold upper-case letters (e.g., \mathbf{A}) denote the matrices. The symbol a_n represents the n th element of vector \mathbf{a} , \mathbf{a}_r indicates the r th column of matrix \mathbf{A} , and a_{nr} stands for the entry in the n th row and r th column of matrix \mathbf{A} . \mathcal{A} denotes a set and its cardinality is indicated by $\#\{\mathcal{A}\}$. The letters \mathbb{R} and \mathbb{C} symbolize the real and complex-valued domain respectively. The operators \mathbf{A}^\top , \mathbf{A}^H , and \mathbf{A}^\dagger correspond to transpose, Hermitian, and pseudo-inverse of matrix \mathbf{A} respectively. The symbol \odot represents Hadamard (element-wise) product. The operations $|\cdot|$, $\|\cdot\|$, and $\|\cdot\|_\text{F}$, indicate absolute value, ℓ_2 -norm, and Frobenius-norm operations respectively. $\exp(\cdot)$ stands for exponential function. $\text{Re}(\cdot)$ and $\text{Im}(\cdot)$ denote the real part and imaginary part of a complex argument respectively. The letter j stands for the imaginary unit, and a^* indicate the complex-conjugate of complex scalar a .

II. SYSTEM MODEL

Consider a co-channel multiuser MIMO downlink system consisting of a BS equipped with N transmit antennas and R RF chains, where $R \ll N$. Let $\mathcal{K} \triangleq \{1, \dots, K\}$ denote a set of K single antenna users served by the BS. The transmit symbol vector at the BS is given by $\mathbf{s} \triangleq [s_1, \dots, s_K]^\top$, where the element s_k indicates the symbol intended for the k th user. The symbols are assumed to be drawn from an M -ary phase-shift keying (M -PSK) constellation², and without loss of generality (w.l.o.g.) each transmit symbol is assumed to be of constant unit modulus. A DP $\mathbf{d}_k \in \mathbb{C}^R$ is applied to the transmit symbol s_k and the resulting signals are fed to the R RF chains. Each RF chain is connected to all transmit antennas through analog PSs. The PSs have constant gains and w.l.o.g. they are assumed to be a same value a for all PSs. Let ρ_{nr} denote the designed (intended) phase value of the PS that connects the n th antenna to the r th RF chain, and $a_{nr} = a \exp(j\rho_{nr})$ denotes the resulting complex value of the corresponding PS. Moreover, $\mathbf{a}_r \triangleq [a_{1r}, \dots, a_{Nr}]^\top$ forms the AP applied to the output of the r th RF chain for $r \in \mathcal{R} \triangleq \{1, \dots, R\}$. Let $\mathbf{A} \triangleq [\mathbf{a}_1, \mathbf{a}_2, \dots, \mathbf{a}_R]$ be the AP matrix. The PSs are assumed to be imperfect, i.e., their actual phase values can vary from their designed phase values due to phase noise, phase drift, etc. [20, 25, 26], while the actual gains of the PSs are unaltered from their nominal values [20, 27]. Let ϕ_{nr} represent the phase error associated with a PS whose designed value is a_{nr} . Then the true value of the PS is given by $a \exp(j(\rho_{nr} + \phi_{nr})) = a_{nr} e_{nr}$, where $e_{nr} \triangleq \exp(j\phi_{nr})$ represents the resulting multiplicative complex error associated with the PS. We assume the phase errors are bounded within a known bound δ such that $-\delta \leq \phi_{nr} \leq \delta$ [20], as shown in Fig. 2. Let the set \mathcal{E} denote the infinite set of all possible error matrices that are associated with the AP matrix \mathbf{A} , i.e.,

$$\mathcal{E} \triangleq \{\mathbf{E} \mid \mathbf{E} \in \mathbb{C}^{N \times R}, |e_{nr}| = 1, |\angle e_{nr}| \leq \delta, \forall n \in \mathcal{N}, \forall r \in \mathcal{R}\}.$$

¹In symbol-level precoding, the precoders are updated at every symbol-interval, whereas, in block-level precoding the precoders are kept constant for a block of symbol-intervals.

²Nevertheless, the proposed techniques can be extended to other modulation formats following the principles in [23, 24].

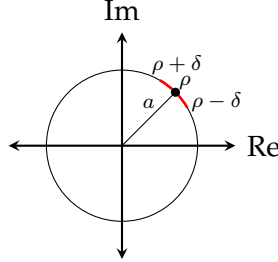


Fig. 2: Phase error around the designed value of a PS.

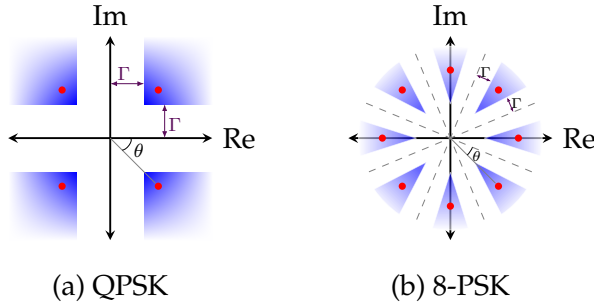


Fig. 3: Constructive interference-regions (in blue shaded area) of constellation symbols.

Let $\tilde{\mathbf{h}}_k \in \mathbb{C}^N$ be the frequency-flat channel vector between the BS and the k th user, which is assumed to be known at the BS [28, 29]. Let $n_k \sim \mathcal{CN}(0, \sigma_k^2)$ represent the i.i.d. additive white Gaussian noise at the k th user. The received signal y_k at the k th user can be expressed as

$$y_k = \tilde{\mathbf{h}}_k^T (\mathbf{A} \odot \mathbf{E}) \left(\sum_{\ell=1}^K \mathbf{d}_\ell s_\ell \right) + n_k, \quad (1)$$

where the error matrix $\mathbf{E} \in \mathcal{E}$.

III. PROBLEM FORMULATION

In a communication system with i.i.d. transmit symbols, the Bayesian decision-region of a symbol for the purpose of decoding is defined as the set of points in the complex domain that have the smallest Euclidean distance to the respective symbol [30]. The CI-based precoding is a linear precoding technique that exploits the knowledge of the channel and data of all users to pre-equalize the transmit signals, such that the received signal at each user lie in the correct decision-region with at-least a *threshold-margin* away from the corresponding decision boundaries [13, 14, 31]. The part of a decision-region that is a threshold-margin away from the corresponding decision boundaries is called as *constructive interference-region* (CI-region). The CI-regions of constellation symbols in the case of QPSK and 8-PSK are illustrated in Fig. 3, where Γ represents the threshold-margin. The enforced threshold-margins control the achieved symbol-error-rates (SERs) and hence the resulting QoS at the users.

In this paper, we extend the CI-based precoding concept to the hybrid precoding architecture. Our objective is to design HPs with the minimum transmit power at the BS,

such that the received signals at each user lie in the CI-regions of the respective transmitted symbols. Note that, when the non-robust precoding is employed, the phase errors in the PSs can drive the received signals at the users outside the corresponding CI-regions, resulting in increased SER. To overcome this drawback, we incorporate robustness into the digital precoding to ensure that the received signal at each user lie in the appropriate CI-region for any error matrix $\mathbf{E} \in \mathcal{E}$. Extending the CI-based precoding problem developed for fully-digital precoding system in [13], we formulate a semi-infinite program [32–34] to implement the above stated task as

$$\underset{\mathbf{A}, \{\mathbf{d}_k\}_{k \in \mathcal{K}}}{\text{minimize}} \left\| \mathbf{A} \sum_{k=1}^K \mathbf{d}_k s_k \right\|^2 \quad (2a)$$

$$\text{s. t. } \left| \text{Im} \left(s_k^* \tilde{\mathbf{h}}_k^T (\mathbf{A} \odot \mathbf{E}) \sum_{\ell=1}^K \mathbf{d}_\ell s_\ell \right) \right| \leq \left(\text{Re} \left(s_k^* \tilde{\mathbf{h}}_k^T (\mathbf{A} \odot \mathbf{E}) \sum_{\ell=1}^K \mathbf{d}_\ell s_\ell \right) - \gamma_k \right) \tan \theta, \quad \forall \mathbf{E} \in \mathcal{E}, \forall k \in \mathcal{K}, \quad (2b)$$

$$|a_{nr}| = a, \quad \forall n \in \mathcal{N}, \forall r \in \mathcal{R}. \quad (2c)$$

In the above problem $\theta \triangleq \pi/M$ denotes the angular distance between the transmit symbol and the corresponding decision boundaries for a given modulation order M , the QoS controlling parameter $\gamma_k \triangleq \Gamma_k / \sin \theta$ with Γ_k indicating the threshold-margin at the k th user. In the problem, the objective function (2a) minimizes the total transmit power at the BS. The constraints in (2b) enforce the received signals to lie in the appropriate CI-regions for each user [13] $\forall \mathbf{E} \in \mathcal{E}$. The constraints in (2c) enforce the constant gain of each element of the AP matrix \mathbf{A} . The problem (2) can be reformulated as an equivalent single-group multicast problem [13, 35] as

$$\underset{\mathbf{A}, \mathbf{b}}{\text{minimize}} \left\| \mathbf{A} \mathbf{b} \right\|^2 \quad (3a)$$

$$\text{s. t. } \left| \text{Im} \left(\mathbf{h}_k^T (\mathbf{A} \odot \mathbf{E}) \mathbf{b} \right) \right| \leq \left(\text{Re} \left(\mathbf{h}_k^T (\mathbf{A} \odot \mathbf{E}) \mathbf{b} \right) - \gamma_k \right) \tan \theta, \quad \forall \mathbf{E} \in \mathcal{E}, \forall k \in \mathcal{K}, \quad (3b)$$

$$|a_{nr}| = a, \quad \forall n \in \mathcal{N}, \forall r \in \mathcal{R}, \quad (3c)$$

where the effective channel $\mathbf{h}_k \triangleq \tilde{\mathbf{h}}_k s_k^*$. The optimal multicast DP \mathbf{b}^* of problem (3) and the optimal DPs \mathbf{d}_k^* of problem (2) are related by [13]

$$\mathbf{d}_k^* = \frac{\mathbf{b}^* s_k^*}{K}, \quad \forall k \in \mathcal{K}. \quad (4)$$

The problem (3) is nonconvex and difficult to solve optimally, due to the following reasons: i) bilinear coupling of AP matrix \mathbf{A} and the DP \mathbf{b} , ii) the nonconvex domain of the elements of \mathbf{A} , iii) the constraint in (3b) must be satisfied $\forall \mathbf{E} \in \mathcal{E}$. i.e., the number of constraints is infinite. We propose a sequential optimization approach that decomposes the problem into two subproblems, namely, analog precoding and robust digital precoding. In Section IV and V, we consider the robust digital precoding and its efficient implementation

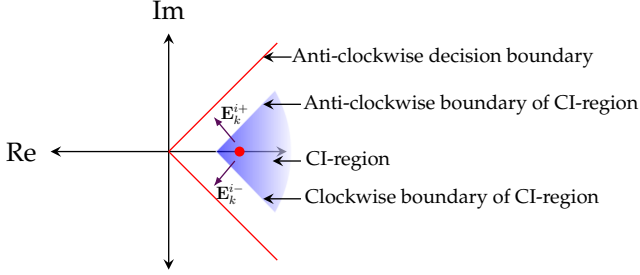


Fig. 4: Anti-clockwise and clockwise drifts of the received signals from the CI-region.

under the premise that the AP matrix is fixed. Subsequently in Section VI we study the AP design techniques.

IV. OPTIMAL ROBUST DIGITAL PRECODING

In this section we design the worst-case robust DP \mathbf{b}^* of problem (3) when the AP matrix \mathbf{A} is fixed to $\hat{\mathbf{A}}$. The resulting problem can be expressed as a semi-infinite problem given by,

$$\underset{\mathbf{b}}{\text{minimize}} \quad \|\hat{\mathbf{A}}\mathbf{b}\|^2 \quad (5a)$$

$$\begin{aligned} \text{s. t. } & +\text{Im}(\mathbf{h}_k^T(\hat{\mathbf{A}} \odot \mathbf{E})\mathbf{b}) \leq \\ & \left(\text{Re}(\mathbf{h}_k^T(\hat{\mathbf{A}} \odot \mathbf{E})\mathbf{b}) - \gamma_k \right) \tan \theta, \quad \forall \mathbf{E} \in \mathcal{E}, \forall k \in \mathcal{K}, \quad (5b) \\ & -\text{Im}(\mathbf{h}_k^T(\hat{\mathbf{A}} \odot \mathbf{E})\mathbf{b}) \leq \\ & \left(\text{Re}(\mathbf{h}_k^T(\hat{\mathbf{A}} \odot \mathbf{E})\mathbf{b}) - \gamma_k \right) \tan \theta, \quad \forall \mathbf{E} \in \mathcal{E}, \forall k \in \mathcal{K}, \quad (5c) \end{aligned}$$

where the constraints in (5b) enforce the received signal at each user to lie below the anti-clockwise boundary of the corresponding CI-region, and the constraints in (5c) enforce them to lie above the clockwise boundary of the corresponding CI-region $\forall \mathbf{E} \in \mathcal{E}$ (see Fig. 4). We assume the problem (5) is feasible. Based on the *cutting plane method and alternating procedure* [33, 34], we develop an iterative algorithm to efficiently solve the formulated semi-infinite program by exploiting a structure in the problem, namely, the constant magnitude property of elements of error matrix $\mathbf{E} \in \mathcal{E}$.

We initialize the algorithm (iteration number $i = 1$) with sets $\mathcal{E}_k^{i+} = \{\mathbf{1}\}$ and $\mathcal{E}_k^{i-} = \{\mathbf{1}\}$, $\forall k \in \mathcal{K}$, where $\mathbf{1}$ is an $N \times R$ matrix with all elements equal to 1. The proposed algorithm comprises two stages in each iteration. In the first stage of the i th iteration we solve the following convex quadratic problem, which corresponds to the non-robust precoding problem in the first iteration.

$$\min_{\mathbf{b}^i} \quad \|\hat{\mathbf{A}}\mathbf{b}^i\|^2 \quad (6a)$$

$$\begin{aligned} \text{s. t. } & +\text{Im}(\mathbf{h}_k^T(\hat{\mathbf{A}} \odot \mathbf{E})\mathbf{b}^i) \leq \\ & \left(\text{Re}(\mathbf{h}_k^T(\hat{\mathbf{A}} \odot \mathbf{E})\mathbf{b}^i) - \gamma_k \right) \tan \theta, \quad \forall \mathbf{E} \in \mathcal{E}_k^{i+}, \forall k \in \mathcal{K}, \quad (6b) \end{aligned}$$

$$\begin{aligned} & -\text{Im}(\mathbf{h}_k^T(\hat{\mathbf{A}} \odot \mathbf{E})\mathbf{b}^i) \leq \\ & \left(\text{Re}(\mathbf{h}_k^T(\hat{\mathbf{A}} \odot \mathbf{E})\mathbf{b}^i) - \gamma_k \right) \tan \theta, \quad \forall \mathbf{E} \in \mathcal{E}_k^{i-}, \forall k \in \mathcal{K}. \quad (6c) \end{aligned}$$

In the subsequent iterations, this problem comprises a finite subset of constraints of problem (5): the constraint (6b) for every error matrix $\mathbf{E} \in \mathcal{E}_k^{i+}$; the constraint (6c) for every error matrix $\mathbf{E} \in \mathcal{E}_k^{i-}$, $\forall k \in \mathcal{K}$. The problem (6) can be solved optimally using any general purpose solver such as SDPT3 [36]. In Section V we develop a customized scheme to solve it more efficiently. Let \mathbf{b}^{i*} denote the optimal solution of the problem (6) in the i th iteration.

In the second stage of the i th iteration, we compute the *worst-case error matrices* of constraints (5b) and (5c) at $\mathbf{b} = \mathbf{b}^{i*}$, $\forall k \in \mathcal{K}$. The worst-case error matrix \mathbf{E}_k^{i+} of constraint (5b) is defined as an error matrix $\mathbf{E} \in \mathcal{E}$ that violates the constraint (5b) with the largest margin, or fulfills it with the smallest margin when the constraint is satisfied $\forall \mathbf{E} \in \mathcal{E}$, for the k th user at $\mathbf{b} = \mathbf{b}^{i*}$. Equivalently, the error matrix $\mathbf{E}_k^{i+} \in \mathcal{E}$ causes the received signal y_k at the k th user furthest away from the CI-region in the anti-clockwise direction (see Fig. 4), when the DP is set to \mathbf{b}^{i*} . Similarly, the worst-case error matrix of constraint (5c) for the k th user, denoted as \mathbf{E}_k^{i-} , drives the received signal y_k furthest away from the corresponding CI-region in the clockwise direction. The closed-form expressions to compute \mathbf{E}_k^{i+} and \mathbf{E}_k^{i-} are presented below. Now, if \mathbf{E}_k^{i+} violates the constraint (5b) then it will be added to the corresponding set of error matrices, i.e.,

$$\mathcal{E}_k^{(i+1)+} = \mathcal{E}_k^{i+} \cup \mathbf{E}_k^{i+}. \quad (7)$$

Similarly, if the error matrix \mathbf{E}_k^{i-} violates the constraint (5c), then it will be included in set $\mathcal{E}_k^{(i+1)-}$, i.e.,

$$\mathcal{E}_k^{(i+1)-} = \mathcal{E}_k^{i-} \cup \mathbf{E}_k^{i-}. \quad (8)$$

When both \mathbf{E}_k^{i+} and \mathbf{E}_k^{i-} , $\forall k \in \mathcal{K}$, satisfy the constraints (5b) and (5c) respectively, we conclude that the solution of problem (6) is the global optimal solution of problem (5) and thus terminate the algorithm.

Optionally, in order to reduce the number of constraints of problem (6) in the next iteration, the redundant constraints can be dropped [34]. To this end, we identify the error matrices $\mathbf{E} \in \mathcal{E}_k^{i+}$ that result in strict inequality of the corresponding constraint in (6b) for the given DP \mathbf{b}^{i*} and exclude them from the set \mathcal{E}_k^{i+} . Similarly, the error matrices $\mathbf{E} \in \mathcal{E}_k^{i-}$ that cause strict inequality of the corresponding constraint in (6c) are excluded from the set \mathcal{E}_k^{i-} .

Closed-form expressions for the worst-case error matrices: The worst-case error matrices, \mathbf{E}_k^{i+} and \mathbf{E}_k^{i-} for $k \in \mathcal{K}$, of constraints (5b) and (5c) for a given DP \mathbf{b}^{i*} can be obtained by solving the problems (9) and (10) respectively. These problems are nonconvex due to the nonconvex domain of optimization variables e_{nr} , $\forall n \in \mathcal{N}$, $\forall r \in \mathcal{R}$. We exploit the constant magnitude property of element e_{nr} and derive a closed-form expression to the worst-case error matrices (see Appendix A), which are given by

$$\mathbf{E}_k^{i+} = \mathbf{U}^+ + j\mathbf{W}^+, \quad (11a)$$

$$\mathbf{E}_k^{i-} = \mathbf{U}^- + j\mathbf{W}^-, \quad (11b)$$

$$\mathbf{E}_k^{i+} = \underset{|e_{nr}|=1, |\angle e_{nr}| \leq \delta}{\operatorname{argmax}} \left(+ \operatorname{Im} \left(\mathbf{h}_k^T (\hat{\mathbf{A}} \odot \mathbf{E}) \mathbf{b}^{i*} \right) - \left(\operatorname{Re} \left(\mathbf{h}_k^T (\hat{\mathbf{A}} \odot \mathbf{E}) \mathbf{b}^{i*} \right) - \gamma_k \right) \tan \theta \right). \quad (9)$$

$$\mathbf{E}_k^{i-} = \underset{|e_{nr}|=1, |\angle e_{nr}| \leq \delta}{\operatorname{argmax}} \left(- \operatorname{Im} \left(\mathbf{h}_k^T (\hat{\mathbf{A}} \odot \mathbf{E}) \mathbf{b}^{i*} \right) - \left(\operatorname{Re} \left(\mathbf{h}_k^T (\hat{\mathbf{A}} \odot \mathbf{E}) \mathbf{b}^{i*} \right) - \gamma_k \right) \tan \theta \right). \quad (10)$$

where the elements of above matrices are computed as

$$u_{nr}^+ = \max \left(\cos \delta, \frac{\operatorname{Im}(z_{nr}) \cos \theta - \operatorname{Re}(z_{nr}) \sin \theta}{|z_{nr}|} \right), \quad (12a)$$

$$w_{nr}^+ = \frac{\operatorname{Re}(z_{nr}) + \operatorname{Im}(z_{nr}) \tan \theta}{|\operatorname{Re}(z_{nr}) + \operatorname{Im}(z_{nr}) \tan \theta|} \sqrt{1 - (u_{nr}^+)^2}, \quad (12b)$$

$$u_{nr}^- = \max \left(\cos \delta, \frac{-\operatorname{Im}(z_{nr}) \cos \theta - \operatorname{Re}(z_{nr}) \sin \theta}{|z_{nr}|} \right), \quad (12c)$$

$$w_{nr}^- = \frac{-\operatorname{Re}(z_{nr}) + \operatorname{Im}(z_{nr}) \tan \theta}{|-\operatorname{Re}(z_{nr}) + \operatorname{Im}(z_{nr}) \tan \theta|} \sqrt{1 - (u_{nr}^-)^2}, \quad (12d)$$

with $\mathbf{Z} \triangleq \left(\mathbf{h}_k (\mathbf{b}^{i*})^T \right) \odot \hat{\mathbf{A}}$. (Indices k and i are dropped from the matrices \mathbf{U}^+ , \mathbf{W}^+ , \mathbf{U}^- , \mathbf{W}^- , and \mathbf{Z} for notational simplicity).

Substituting the optimal solutions \mathbf{E}_k^{i+} and \mathbf{E}_k^{i-} in the objective functions of the problems (9) and (10) we obtain the optimal values v_k^{i+} and v_k^{i-} respectively. A non-positive v_k^{i+} implies that \mathbf{b}^{i*} satisfies the constraint (5b) for the k th user $\forall \mathbf{E} \in \mathcal{E}$. On the other hand, a positive value for v_k^{i+} implies that the constraint (5b) is violated at $\mathbf{b} = \mathbf{b}^{i*}$ for the error matrix \mathbf{E}_k^{i+} ; a positive v_k^{i-} means the constraint (5c) is violated at $\mathbf{b} = \mathbf{b}^{i*}$ for the error matrix \mathbf{E}_k^{i-} , for the k th user.

The above algorithm to design the worst-case robust digital precoding is summarized in Alg. 1.

Algorithm 1: Optimal robust digital precoding

- 1: Initialize $i = 1$, $\mathcal{E}_k^{i+} = \{\mathbf{1}\}$, $\mathcal{E}_k^{i-} = \{\mathbf{1}\}$, $\forall k \in \mathcal{K}$.
- 2: **loop**
- 3: Compute \mathbf{b}^{i*} by solving problem (6) [e.g., using the proposed scheme in Section VI].
- 4: Compute \mathbf{E}_k^{i+} and \mathbf{E}_k^{i-} using Eq. (11a) and Eq. (11b) respectively, $\forall k \in \mathcal{K}$.
- 5: Substitute \mathbf{E}_k^{i+} and \mathbf{E}_k^{i-} in the objective functions of the problems (9) and (10) to obtain the corresponding optimal values v_k^{i+} and v_k^{i-} respectively.
- 6: If $v_k^{i+} > 0$ then execute Eq. (7), and if $v_k^{i-} > 0$ then execute Eq. (8), $\forall k \in \mathcal{K}$.
- 7: **Break**, if both v_k^{i+} and v_k^{i-} are non-positive $\forall k \in \mathcal{K}$.
- 8: $i \leftarrow i + 1$.
- 9: **end loop**

Theorem 1: When Alg. 1 terminates after an I th iteration the optimal solution \mathbf{b}^{I*} of problem (6) is equal to the optimal solution \mathbf{b}^* of problem (5).

Proof: see Appendix B-1.

Theorem 2: The sequence, $\mathbf{b}^{1*}, \mathbf{b}^{2*}, \dots$, of optimal solutions of problem (6) generated by Alg. 1 converges to the optimal solution \mathbf{b}^* of problem (5).

Proof: see Appendix B-2.

V. LOW-COMPLEXITY PARALLEL IMPLEMENTATION SCHEME

The major part of the computations involved in the proposed robust digital precoding algorithm is contributed from the optimization problem (6), which needs to be solved in every iteration. In this section we develop a low-complexity scheme, which can solve the problem (6) in a parallelized manner in order to reap the benefits of any available parallel hardwares and thus speed up the algorithm.

In the following, firstly we transform the complex-valued problem (6) into an equivalent real-valued problem and then derive its dual problem. Subsequently, the dual problem is solved iteratively, as similar in [37, 38], to obtain the optimal solution of the primal problem by performing the following steps: first, an approximate problem is constructed for the dual problem that delivers a descent direction of the dual problem at a given point. Next, the approximate problem is decomposed into multiple independent subproblems, which can be solved in parallel. Afterwards, a closed-form expression is derived for the optimal solutions of the subproblems. Finally we derive a closed-form expression to compute the step-size, which is required to update the current point in the descent direction.

Let $\mathcal{F}_{c2r}(\mathbf{X})$ be a function that transforms a complex matrix \mathbf{X} to a real matrix \mathbf{Y} such that

$$\mathbf{Y} = \mathcal{F}_{c2r}(\mathbf{X}) \triangleq \begin{bmatrix} \operatorname{Re}(\mathbf{X}), -\operatorname{Im}(\mathbf{X}) \\ \operatorname{Im}(\mathbf{X}), \operatorname{Re}(\mathbf{X}) \end{bmatrix}. \quad (13)$$

Let $f_{c2r}(\mathbf{x})$ be a function that transforms a complex vector \mathbf{x} into a real vector \mathbf{y} such that

$$\mathbf{y} = f_{c2r}(\mathbf{x}) \triangleq [\operatorname{Re}(\mathbf{x})^T, \operatorname{Im}(\mathbf{x})^T]^T. \quad (14)$$

Let $\mathbf{M}_0 \triangleq \mathcal{F}_{c2r}(\hat{\mathbf{A}})$. We define the sets of AP matrices of problem (6) in real-valued domain as below (the iteration index i is dropped for notational convenience).

$$\mathcal{M}_k^+ \triangleq \{\mathbf{M} = \mathcal{F}_{c2r}(\hat{\mathbf{A}} \odot \mathbf{E}) \mid \mathbf{E} \in \mathcal{E}_k^+\}, \quad \forall k \in \mathcal{K}, \quad (15)$$

$$\mathcal{M}_k^- \triangleq \{\mathbf{M} = \mathcal{F}_{c2r}(\hat{\mathbf{A}} \odot \mathbf{E}) \mid \mathbf{E} \in \mathcal{E}_k^-\}, \quad \forall k \in \mathcal{K}. \quad (16)$$

Furthermore we define the following: $\mathbf{g} \triangleq f_{c2r}(\mathbf{b})$, $\mathbf{f}_k \triangleq f_{c2r}(\mathbf{h}_k)$, and

$$\mathbf{\Pi}_1 \triangleq \begin{bmatrix} \mathbf{I}, & \mathbf{0} \\ \mathbf{0}, & -\mathbf{I} \end{bmatrix}, \quad \mathbf{\Pi}_2 \triangleq \begin{bmatrix} \mathbf{0}, & \mathbf{I} \\ \mathbf{I}, & \mathbf{0} \end{bmatrix}, \quad (17)$$

$$\mathbf{p}_k \triangleq \mathbf{\Pi}_2 \mathbf{f}_k, \quad \mathbf{q}_k \triangleq \mathbf{\Pi}_1 \mathbf{f}_k \tan \theta, \quad r_k \triangleq \gamma_k \tan \theta. \quad (18)$$

In Eq. (17), \mathbf{I} and $\mathbf{0}$ are $N \times N$ identity and zero matrices respectively. Now we can reformulate the problem (6) in real-valued domain as

$$\underset{\mathbf{g}}{\operatorname{minimize}} \quad \|\mathbf{M}_0 \mathbf{g}\|^2 \quad (19)$$

$$\text{s. t. } (+\mathbf{p}_k - \mathbf{q}_k)^T \mathbf{M} \mathbf{g} + r_k \leq 0, \quad \forall \mathbf{M} \in \mathcal{M}_k^+, \forall k \in \mathcal{K},$$

$$(-\mathbf{p}_k - \mathbf{q}_k)^T \mathbf{M} \mathbf{g} + r_k \leq 0, \quad \forall \mathbf{M} \in \mathcal{M}_k^-, \forall k \in \mathcal{K}.$$

The Lagrangian function of the above problem can be written as

$$\mathcal{L}(\mathbf{g}, \boldsymbol{\lambda}) = \|\mathbf{M}_0 \mathbf{g}\|^2 - (\boldsymbol{\Psi} \boldsymbol{\lambda})^\top \mathbf{g} + \mathbf{r}^\top \boldsymbol{\lambda}, \quad (20)$$

where $\boldsymbol{\lambda}$ denotes the vector of Lagrange multipliers. The matrix $\boldsymbol{\Psi}$ and vector \mathbf{r} are given in Eq. (21) and Eq. (22) respectively.

Taking the infimum of the Lagrangian function $\mathcal{L}(\mathbf{g}, \boldsymbol{\lambda})$ w.r.t. \mathbf{g} we obtain the dual function in terms of $\boldsymbol{\lambda}$, and subsequently we formulate the dual problem of (19) as

$$\underset{\boldsymbol{\lambda}}{\text{minimize}} \quad \|\mathbf{N} \boldsymbol{\lambda}\|^2 - \mathbf{r}^\top \boldsymbol{\lambda} \quad (23a)$$

$$\text{s. t. } \boldsymbol{\lambda} \geq \mathbf{0}, \quad (23b)$$

where $\mathbf{N} \triangleq \frac{(\mathbf{M}_0^\dagger)^\top \boldsymbol{\Psi}}{2}$. Note that the problem (19) is convex and it comprises only affine inequalities in \mathbf{g} . Therefore, according to the Slater's condition strong duality holds for this problem when it is feasible [39]. Moreover, one of the KKT conditions dictates that the Lagrangian function (20) has a vanishing gradient w.r.t. \mathbf{g} at an optimal primal point \mathbf{g}^* and an optimal dual point $\boldsymbol{\lambda}^*$ [39]. By setting $\frac{\partial \mathcal{L}(\mathbf{g}^*, \boldsymbol{\lambda}^*)}{\partial \mathbf{g}} = 0$ we obtain the expression for an optimal primal point \mathbf{g}^* of the problem (19) in terms of the corresponding optimal dual point $\boldsymbol{\lambda}^*$ as

$$\mathbf{g}^* = \frac{(\mathbf{M}_0^\top \mathbf{M}_0)^{-1}}{2} \boldsymbol{\Psi} \boldsymbol{\lambda}^*. \quad (24)$$

In the following we design an iterative algorithm to solve the dual problem (23) optimally.

Approximate problem: Let W be the total number of elements in vector $\boldsymbol{\lambda}$ and $\mathcal{W} \triangleq \{1, \dots, W\}$. In problem (23) the objective function is convex in each variable λ_w for $w \in \mathcal{W}$. Therefore, based on the Jacobi theorem [37, 40] we construct an approximate problem for the problem (23) in the i th iteration around a given point $\boldsymbol{\lambda}^i$ as

$$\underset{\lambda_w, w \in \mathcal{W}}{\text{minimize}} \quad \sum_{w=1}^W \left(\|\mathbf{N}_{-w} \boldsymbol{\lambda}_{-w}^i + \mathbf{n}_w \lambda_w\|^2 - \mathbf{r}_{-w}^\top \boldsymbol{\lambda}_{-w}^i - r_w \lambda_w \right) \quad (25a)$$

$$\text{s. t. } \lambda_w \geq 0, \quad \forall w \in \mathcal{W}, \quad (25b)$$

where \mathbf{N}_{-w} denotes the matrix obtained by discarding the w th column \mathbf{n}_w from matrix \mathbf{N} , $\boldsymbol{\lambda}_{-w}^i$ denotes the vector obtained by discarding the w th element from vector $\boldsymbol{\lambda}^i$, and \mathbf{r}_{-w} denotes the vector obtained by eliminating the w th element r_w from vector \mathbf{r} . Let $\hat{\boldsymbol{\lambda}} \triangleq [\hat{\lambda}_1, \dots, \hat{\lambda}_W]^\top$ denote the optimal solution of this problem. Then, according to the Jacobi theorem $\hat{\boldsymbol{\lambda}} - \boldsymbol{\lambda}^i$ represents a descent direction of the objective function (23a) in the domain of problem (23) [37, 40]. Therefore, the current point $\boldsymbol{\lambda}^i$ can be updated in the descent direction of the objective function (23a) as

$$\boldsymbol{\lambda}^{i+1} = \boldsymbol{\lambda}^i + \eta^i (\hat{\boldsymbol{\lambda}} - \boldsymbol{\lambda}^i), \quad (26)$$

where η^i is an appropriate step-size, with $0 < \eta^i \leq 1$. When $\hat{\boldsymbol{\lambda}} = \boldsymbol{\lambda}^i$ the iterative algorithm has converged to the global optimal solution $\boldsymbol{\lambda}^*$ of problem (23).

Decomposition of the approximate problem: The objective function (25a) comprises W summands, where each summand contains only one optimization variable λ_w . Moreover, the

constraints set in (25b) is a Cartesian product of W convex sets, with each convex set defined by only one optimization variable λ_w . Therefore we can decompose the problem (25) into W independent subproblems [37], each involving only one optimization variable λ_w , as

$$\hat{\lambda}_w = \underset{\lambda_w \geq 0}{\text{argmin}} \quad \|\mathbf{N}_{-w} \boldsymbol{\lambda}_{-w}^i + \mathbf{n}_w \lambda_w\|^2 - r_w \lambda_w, \quad (27)$$

$\forall w \in \mathcal{W}$, where the constant term $\mathbf{r}_{-w}^\top \boldsymbol{\lambda}_{-w}^i$ has been dropped without affecting the optimal solution.

Closed-form solution of the subproblems: The objective function in subproblem (27) is convex in λ_w , and it comprises only an affine inequality, namely, $\lambda_w \geq 0$. According to Slater's condition the strong duality holds for the subproblem and its dual, and KKT conditions are satisfied by the primal and dual optimal points of the subproblem [39]. The Lagrangian of subproblem (27) can be written as

$$\mathcal{L}(\lambda_w, \mu_w) = \|\mathbf{N}_{-w} \boldsymbol{\lambda}_{-w}^i + \mathbf{n}_w \lambda_w\|^2 - r_w \lambda_w - \mu_w \lambda_w, \quad (28)$$

where μ_w is the Lagrange multiplier. Using the KKT conditions we derive a closed-form expression for $\hat{\lambda}_w$ as

$$\hat{\lambda}_w = \max \left(0, \frac{1}{\|\mathbf{n}_w\|^2} \left(\frac{r_w}{2} - \mathbf{n}_w^\top \mathbf{N}_{-w} \boldsymbol{\lambda}_{-w}^i \right) \right). \quad (29)$$

Optimal step-size computation: Based on the exact line search method [37], we can formulate an optimization problem to compute the optimal step-size η^i that minimizes the objective function (23a) between the current point $\boldsymbol{\lambda}^i$ and the descent direction $\hat{\boldsymbol{\lambda}}$ as

$$\eta^i = \underset{0 \leq \eta \leq 1}{\text{argmin}} \quad \underbrace{\left\| \mathbf{N} (\boldsymbol{\lambda}^i + \eta (\hat{\boldsymbol{\lambda}} - \boldsymbol{\lambda}^i)) \right\|^2 - \mathbf{r}^\top (\boldsymbol{\lambda}^i + \eta (\hat{\boldsymbol{\lambda}} - \boldsymbol{\lambda}^i))}_{\hat{f}(\eta)}. \quad (30)$$

The function $\hat{f}(\eta)$ in the above problem is convex and differentiable in η . Differentiating $\hat{f}(\eta)$ w.r.t. η and equating the gradient to zero, we obtain a closed-form expression for the optimal solution η^i of problem (30) as

$$\eta^i = \left[\frac{-2(\mathbf{N} \boldsymbol{\lambda}^i)^\top \mathbf{N} (\hat{\boldsymbol{\lambda}} - \boldsymbol{\lambda}^i) + \mathbf{r}^\top (\hat{\boldsymbol{\lambda}} - \boldsymbol{\lambda}^i)}{2 (\mathbf{N} (\hat{\boldsymbol{\lambda}} - \boldsymbol{\lambda}^i))^\top \mathbf{N} (\hat{\boldsymbol{\lambda}} - \boldsymbol{\lambda}^i)} \right]_0^1. \quad (31)$$

Termination: When $\hat{\boldsymbol{\lambda}} = \boldsymbol{\lambda}^i$ the iterative algorithm has converged to the global optimal solution of problem (23) [37]. In practical applications where a finite numerical precision is sufficient, the iterations can be terminated when $\|\boldsymbol{\lambda}^{(i+1)} - \boldsymbol{\lambda}^{(i)}\| \leq \varepsilon$, where ε is a small positive scalar that controls the numerical precision of the scheme.

The above proposed scheme to solve the problem (6) is summarized in Alg. 2.

VI. BLOCK-LEVEL ANALOG PRECODING

In the previous sections we focused on designing the DPs under the premise that APs are fixed. In this section we discuss techniques to design APs in CI-based hybrid precoding setting.

$$\Psi \triangleq \left[(\mathbf{M}_{1,1}^+)^T (\mathbf{q}_1 - \mathbf{p}_1), \dots, (\mathbf{M}_{1,L_1^+}^+)^T (\mathbf{q}_1 - \mathbf{p}_1), \dots, (\mathbf{M}_{K,1}^+)^T (\mathbf{q}_K - \mathbf{p}_K), \dots, (\mathbf{M}_{K,L_K^+}^+)^T (\mathbf{q}_K - \mathbf{p}_K), \right. \\ \left. (\mathbf{M}_{1,1}^-)^T (\mathbf{q}_1 + \mathbf{p}_1), \dots, (\mathbf{M}_{1,L_1^-}^-)^T (\mathbf{q}_1 + \mathbf{p}_1), \dots, (\mathbf{M}_{K,1}^-)^T (\mathbf{q}_K + \mathbf{p}_K), \dots, (\mathbf{M}_{K,L_K^-}^-)^T (\mathbf{q}_K + \mathbf{p}_K) \right], \quad (21)$$

$$\mathbf{r} \triangleq [r_1 \mathbf{1}^{1 \times L_1^+}, \dots, r_K \mathbf{1}^{1 \times L_K^+}, r_1 \mathbf{1}^{1 \times L_1^-}, \dots, r_K \mathbf{1}^{1 \times L_K^-}]^T, \quad (22)$$

where $\mathbf{M}_{k,m}^+$ is the m th element of set \mathcal{M}_k^+ , $\mathbf{M}_{k,m}^-$ is the m th element of set \mathcal{M}_k^- , $L_k^+ \triangleq \#\{\mathcal{M}_k^+\}$, and $L_k^- \triangleq \#\{\mathcal{M}_k^-\}$.

Algorithm 2: Low-complexity parallel implementation scheme

- 1: Initialize $i = 1$ and $\boldsymbol{\lambda}^{(1)}$ to any non-negative values.
- 2: **loop**
- 3: Compute $\hat{\boldsymbol{\lambda}}$ using Eq. (29) [each element in $\hat{\boldsymbol{\lambda}}$ can be computed independently in parallel].
- 4: Compute step-size η^i using Eq. (31).
- 5: Update the current point to $\boldsymbol{\lambda}^{i+1}$ using Eq. (26).
- 6: **Break**, if $\|\boldsymbol{\lambda}^{(i+1)} - \boldsymbol{\lambda}^{(i)}\| \leq \varepsilon$.
- 7: $i \leftarrow i + 1$.
- 8: **end loop**
- 9: Compute \mathbf{g}^* from $\boldsymbol{\lambda}^*$ using Eq. (24). Obtain \mathbf{b}^* from \mathbf{g}^* using the relation in Eq. (14).

There are two types of APs that are generally used in hybrid precoding systems, namely, continuous-valued APs [7] and codebook-based APs [10, 41]. A continuous-valued AP has more degrees of freedom, as each of its elements can take any phase value between 0 and 2π . However, its realization requires expensive high resolution tunable PSs. On the other hand, in a codebook-based analog precoding the APs are selected from a predefined codebook that is commonly realized in hardware with switchable spatial filter banks composed of inexpensive fixed PSs [42]. Due to the reduced degrees of freedom, the codebook-based APs require an increased transmit power to fulfill a certain QoS as compared to the continuous-valued APs.

Paper [18] compares the performance of different symbol-level AP design techniques in a CI-based hybrid precoding system. These techniques can be used to obtain the AP matrix \mathbf{A} at every symbol-interval before employing the proposed algorithm to compute the robust DPs. However, the symbol-level AP design can become inappropriate in many scenarios, such as ultra-low latency applications of 5G networks having symbol duration requirement of few micro-seconds [19]. In such cases, the symbol-level analog precoding can cause drastic performance degradation in hybrid precoding systems with inexpensive PSs having the transient response time in the order of micro-seconds (e.g., PSs comprising RF MEMS [43]). In order to overcome this shortcoming we propose the block-level analog precoding, where an AP matrix that is suitable for a block of T symbol-intervals is designed, instead of recomputing it in every symbol-interval. We choose $T \leq T_c$, where T_c is the coherence time of the channel, so that the block-level AP matrix can be designed using the known constant channel matrix. In the following we extend the application of methods of [18] to the block-level analog

precoding.

A. Continuous-valued AP design

1) *Conjugate phase of channel (CPC) method*: In this method the BS assigns a dedicated RF chain to each user. Then, the array gain between the k th user and the associated RF chain is maximized by assigning the conjugate phase values of the elements of channel vector $\tilde{\mathbf{h}}_k$ to the corresponding elements of the AP \mathbf{a}_k , i.e., $a_{nk} = ae^{-j\beta_{nk}}$, where β_{nk} indicates the phase value of the n th element of channel vector \mathbf{h}_k [6]. We remark that in this method the AP matrix is independent of transmit symbol vector, and remain same as long as the channel is constant. Thus the method is inherently suitable for block-level AP design.

B. Codebook-based AP design

In the codebook-based AP design techniques, the APs are chosen from a predefined set $\mathcal{C} \triangleq \{\mathbf{c}_1, \dots, \mathbf{c}_C\}$, where $C \geq R$. Let $\mathbf{C} \triangleq [\mathbf{c}_1, \dots, \mathbf{c}_C]$ be the corresponding codebook matrix.

1) *Margin widening and selection operator (MWASO)*: In [18] a sparsity-based AP selection technique, termed as MWASO, is devised to select R APs from the codebook that maximize a utility function of the system. Here, we extend this technique to enable block-level analog precoding over T symbol-intervals by formulating a block-sparsity-based convex optimization problem [44, 45] as

$$\underset{\Upsilon \in \mathbb{R}, \{\mathbf{x}_t\}_{t \in \mathcal{T}}}{\text{minimize}} \quad \Upsilon + \epsilon \|\mathbf{X}\|_{2,1} \quad (32a)$$

$$\text{s. t. } \left| \text{Im} \left(s_k^* \tilde{\mathbf{h}}_k^T \mathbf{C} \mathbf{x}_t \right) \right| \leq \left(\text{Re} \left(s_k^* \tilde{\mathbf{h}}_k^T \mathbf{C} \mathbf{x}_t \right) - (\gamma_k - \Upsilon) \right) \tan \theta, \\ \forall k \in \mathcal{K}, \forall t \in \mathcal{T}. \quad (32b)$$

In this problem, $\gamma_k - \Upsilon$ determines the minimum margin between the received signals and the decision boundaries of the associated transmit symbols of the k th user over all T symbol-intervals. The optimization variable Υ in the objective function along with the constraints in (32b) forces the received signals towards the interior of the CI-region for all K users over all T symbol-intervals. The optimization matrix $\mathbf{X} \triangleq [\mathbf{x}_1, \dots, \mathbf{x}_T] \in \mathbb{C}^{C \times T}$ acts as the selection operator. The mixed $\ell_{2,1}$ norm in the objective function promotes row sparsity on the matrix \mathbf{X} [45], thereby allowing the selection of APs from the codebook matrix \mathbf{C} that are appropriate for all T symbol-intervals. The positive scalar ϵ is an appropriate weighting factor, which can be chosen e.g., using bisection method, to force the number of non-zero rows in \mathbf{X} equal to R . Subsequently, the columns of the codebook matrix \mathbf{C} that

correspond to the non-zero rows of the optimal solution \mathbf{X}^* forms the AP matrix $\hat{\mathbf{A}}$.

2) *Best matching code selection (BMCS) method:* In this method, for each user the AP from the codebook \mathcal{C} that maximizes the inner product with its channel vector is selected [18]. Similar to the CPC method, this method designs the AP matrix independent of the transmit symbol vector, and hence it is inherently suitable for block-level AP design.

After obtaining the block-level AP matrix by employing any appropriate method, we proceed to design the robust DPs at every symbol-interval as discussed in the previous sections.

VII. NUMERICAL RESULTS

In this section, we first evaluate the QoS degradation at the users due to phase errors in PSs in the case of CI-based non-robust hybrid precoding to validate the necessity of the robust hybrid precoding. Then we compare the performance of proposed robust precoding with that of a conventional robust precoding technique. Afterwards, we compare the performance of proposed CI-based hybrid precoding with that of the interference-suppression-based state-of-the-art precoding schemes for non-robust scenarios. Next, we numerically evaluate the performance of different block-level analog precoding methods. Finally, we examine the computational complexity of different methods. For the simulation we employ geometric channel model [6, 46].

In interference-suppression-based precoding systems, the SINR metric is generally used to measure the quality of received signal, as the SINR controls the achieved SER. However, in CI-based precoding systems the interference plays a constructive role and it does not necessarily cause symbol-error; therefore the SINR is not an appropriate metric to measure the quality of received signals in this system. In order to quantify the received signal quality in CI-based precoding in a noisy-environment we introduce a metric *Threshold-margin-to-Noise power Ratio* (TNR), which is defined as $TNR_k \triangleq \frac{\Gamma_k}{\sigma_k^2}$. It measures the relative margin between the CI-region and the corresponding decision boundaries w.r.t. noise power, and directly influences the achieved SER. The empirical relations between SNR, TNR, and SER for different modulation schemes are provided in Appendix C.

A. QoS degradation due to errors in PSs

In order to determine the extent of QoS degradation at the users due to errors in the PSs in CI-based hybrid precoding systems, we employ the non-robust precoding and compute the resulting SER. Table I lists the percentage increase in SER when compared to the expected value (which is achieved in the case of ideal PSs), due to errors in the PSs for different phase error bound δ . The table indicates significant deterioration in QoS, hence reaffirming the need of robust precoding in such scenarios. The proposed robust precoding is designed to handle the worst-case scenario, thus it completely eliminates the symbol-errors resulting from phase errors in PSs (i.e., 0% SER increase).

TABLE I: SER increase vs. phase error bound δ in the case of CI-based non-robust hybrid precoding for $N = 128$, $R = K = 4$, TNR = 2, and QPSK modulation.

Phase error bound δ	2°	4°	6°	8°	10°
SER increase	0.41%	1.34%	2.34%	3.91%	6.72%

B. Proposed vs. conventional robust hybrid precoding

A conventional approach to obtain the robust DPs is to design non-robust DPs targeting a larger QoS than the required QoS. This technique provides robustness against errors by assigning an extra power to the DPs, when compared to the power required to achieve the actual QoS in the error-free scenario [47, 48]. This method can be extended to the CI-based hybrid precoding by appropriately choosing a new TNR value for the non-robust precoding that achieves a similar SER performance in the presence of phase errors in the PSs and additive noise at the users, as that of the optimal worst-case robust DPs. In our simulation we choose the new TNR values using the empirical relation between δ , TNR, and SER given in Table IV of Appendix D.

Table II compares the performance of proposed optimal robust precoding method and the conventional method. For different values of δ we design robust HPs using the proposed algorithm to achieve a TNR = 2, and compute the required transmit power P_{opt} and the resulting SER. Then we compute the TNR value required to achieve a similar SER performance for the given δ with non-robust precoding using Table IV. For this tuned TNR value we design the non-robust DPs and compute the resulting transmit power P_{conv} . Table II reveals that the conventional method requires significantly more transmit power when compared to the optimal robust precoding method.

C. CI-based precoding vs. state-of-the-art precoding schemes

In this subsection we compare the SER achieved by the proposed CI-based hybrid precoding with that of the following state-of-the-art hybrid precoding schemes: the PZF method proposed in [6], interference-suppression-based hybrid precoding method (IS-based HP) proposed in [7].

In the formulated CI-based hybrid precoding problem, the objective is to minimize the transmit power for a given TNR. However, the considered competing methods aim to maximize the spectral efficiency (or SINR) for a given power budget. In order to facilitate a fair comparison, we utilize the empirical relation between SNR, TNR, and SER given in Appendix C, and obtain *SER vs. transmit power* relations for all methods. For the simulation we adopt the following system parameters: $N = 128$ transmit antennas, and $K = 4$ users. We use $R = 4$ RF chains in the case of proposed CI-based hybrid precoding and PZF method, and $R = 5$ for IS-based HP (this method requires $R > K$). The PSs are assumed to be ideal.

Fig. 5 depicts the SER achieved by all three methods for BPSK, QPSK, and 8-PSK modulation schemes. In the figure, we notice that the proposed method considerably reduces the SER when compared to the competing methods for all

TABLE II: Performance comparison of the proposed optimal and the conventional CI-based robust hybrid precoding for $N = 128$, $R = K = 4$, and QPSK modulation.

δ (deg)	Optimal robust		SER	Conventional robust		$\frac{(P_{\text{conv}} - P_{\text{opt}})}{P_{\text{opt}}}$
	TNR	P_{opt} (Watts)		TNR	P_{conv} (Watts)	
1°	2	0.4133	2.5e-3	2.2603	0.4631	12.0%
2°	2	0.4816	1.1e-3	2.4195	0.5280	9.6%
3°	2	0.5695	4.0e-4	2.4989	0.5834	2.4%
4°	2	0.6855	1.0e-4	2.8731	0.7376	7.6%

considered modulation schemes (approx. 500x for BPSK with Transmit power = 5 dB).

D. CI-based hybrid precoding vs. fully-digital precoding

Fig. 6 compares the SER (in log10-scale) achieved by the proposed CI-based hybrid precoding with that of the optimal CI-based fully-digital precoding [13] and conventional SINR fulfillment-based fully-digital precoding [4, 17] (referred to as *Conv. fully-DP*), for a system with $N = 64$ transmit antennas and $K = 8$ users. Both CI-based and SINR fulfillment-based fully-digital precoding assume the number of RF chains $R = N = 64$. The proposed method is employed for different values of R , and the APs are chosen from a 64×64 DFT codebook using MWASO method. The figure also comprises the SER achieved by the CI-based hybrid precoding with continuous-valued APs, which are designed employing the CPC method.

The figure reveals that the CI-based hybrid precoding (even with $R = K$, and codebook-based APs) yields significantly better performance than the conv. SINR fulfillment-based fully-digital precoding. As we increase the number of RF chains, the SER of the CI-based hybrid precoding gradually approaches that of the optimal CI-based fully-digital precoding. Moreover we notice that the continuous-valued analog precoding yields considerably better results than the codebook-based analog precoding at the cost of expensive high resolution PSs.

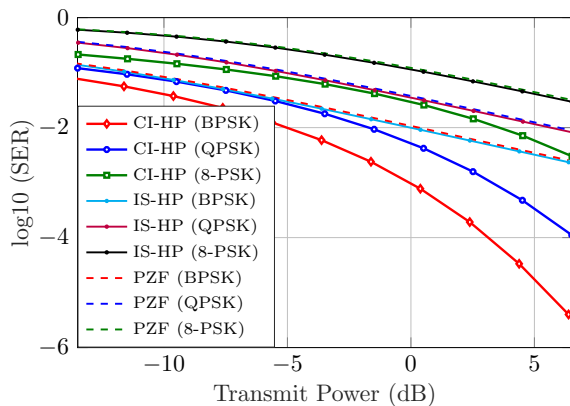


Fig. 5: SER (in log10-scale) comparison of PZF method [6], IS-based HP [7] (IS-HP), and the proposed CI-based hybrid precoding (CI-HP), for $N = 128$, $K = 4$, and QPSK modulation.

E. Evaluation of block-level analog precoding techniques

In this subsection, we compare the performance of different block-level analog precoding techniques in terms of transmit powers of the resulting HPs to achieve a certain QoS. In order to facilitate a fair comparison, the optimal CI-based DPs are designed followed by every block-level analog precoding technique. Fig. 7 plots transmit power of the HPs in different methods over a range of block-length T . The figure also plots the transmit power required in the case of the CI-based fully-digital precoding for comparison. In the simulation we assume the channel is constant for $T_c = 8$ symbol-intervals. As we discussed in Section VI, the CPC and BMCS methods are based on channel matrix and independent of

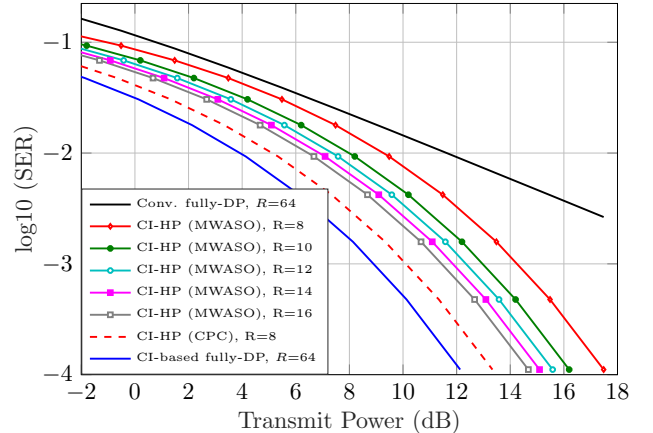


Fig. 6: Performance comparison of the proposed CI-based hybrid precoding (CI-HP), with CI-based and conv. fully-digital precoding for $N = 64$, and $K = 8$.

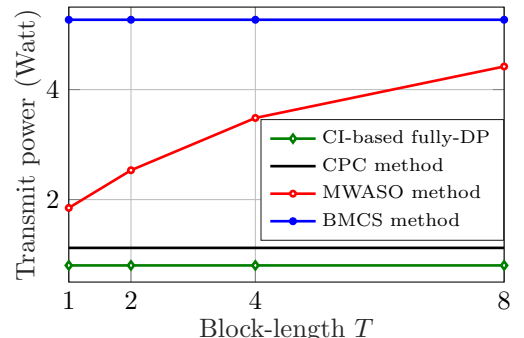


Fig. 7: Comparison of different block-level AP design techniques for $N = 64$, $R = K = 16$, $T_{\text{NR}} = 1$, and $T_c = 8$.

transmit symbols. Therefore, the transmit powers associated with these methods are constant over the block-length T . On the contrary, the MWASO method designs the APs based on both channel matrix and the transmit symbol vector. Thus, the transmit power required by the MWASO method increases with T . The figure also reveals that the continuous-valued CPC method is considerably more efficient than the codebook-based MWASO and BMCS methods in terms of transmit power. The MWASO method results in smaller transmit power, however computationally more demanding as it involves solving an optimization problem, when compared to the heuristic BMCS method.

F. Computational complexity analysis

In this subsection, we evaluate the computational complexity of different methods discussed in this paper in terms of their computational time. The simulations are conducted on a system having the following features: Intel (R) Core (TM) i7-4790K CPU @ 4.00GHz, Arch Linux 4.16.8, MATLAB 2018b, CVX 2.1 with SDPT3 solver.

Table III lists the average computation time required to implement the proposed robust hybrid precoding using CVX with SDPT3 and the proposed scheme (Alg. 2) for different values of phase error bound δ . In the table we notice that the proposed scheme is significantly faster than the SDPT3 solver.

TABLE III: Average computation time (in seconds) to implement the proposed robust hybrid precoding using CVX and the proposed scheme, for $N = 128$, $R = K = M = 4$, and $\text{TNR} = 2$.

δ	0°	1°	2°	3°	4°	5°
CVX	0.30	0.60	0.61	0.65	0.72	0.80
Alg. 2	2.8e-3	9.3e-3	1.3e-2	4.9e-2	9.4e-2	0.10

Fig. 8 plots computation time required by different methods to compute the non-robust HPs for different values of K . The figure reveals that the CI-based HPs can be computed significantly faster using the proposed scheme in Alg. 2 compared to using the CVX with SDPT3. Even though the PZF method is faster when compared to the proposed method, we have seen in Section VII-C that it is inferior to the proposed method in terms of SER performance.

We consider the rigorous theoretical and numerical analysis of computational complexities of different methods and their comparison as our future work.

VIII. CONCLUSION

In this paper we developed an algorithm for computing the optimal CI-based digital precoders with robustness against errors in the PSs. We also devised a scheme to facilitate the implementation of the proposed algorithm efficiently in a distributed manner on parallel hardware architectures. Furthermore we proposed block-level analog precoding techniques, which are necessary for ultra-low latency applications. The simulation results validated the need of the CI-based robust

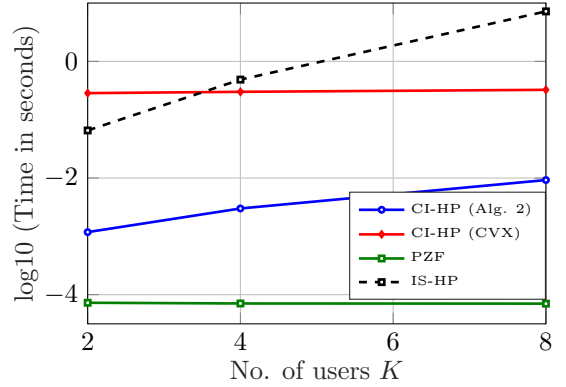


Fig. 8: Computation time (in seconds, log10-scale) vs. No. of users K , for $N = 8K$, $M = 4$, $R = K + 1$ for IS-based HP, and $R = K$ for other methods.

hybrid precoding, and demonstrated the superiority of the proposed precoding over a conventional robust hybrid precoding method. The results illustrated the superiority of the CI-based hybrid precoding when compared to the interference-suppression-based state-of-the-art schemes. We also verified that the devised scheme is significantly faster in implementing the robust precoding when compared to the general purpose solver SDPT3. Furthermore, we inferred from the simulations that the continuous-valued APs yield significantly better performance in block-level precoding, at the cost of high resolution PSs, when compared to the codebook-based APs.

APPENDIX A CLOSED-FORM EXPRESSIONS FOR THE WORST-CASE ERROR MATRICES

Consider the objective function of problem (9)

$$\hat{f} \triangleq \text{Im} \left(\mathbf{h}_k^T (\hat{\mathbf{A}} \odot \mathbf{E}) \mathbf{b}^{i*} \right) - \left(\text{Re} \left(\mathbf{h}_k^T (\hat{\mathbf{A}} \odot \mathbf{E}) \mathbf{b}^{i*} \right) - \gamma_k \right) \tan \theta.$$

Let $g \triangleq \mathbf{h}_k^T (\hat{\mathbf{A}} \odot \mathbf{E}) \mathbf{b}^{i*}$. We can rewrite g as,

$$g = \sum_{\forall n \in \mathcal{N}} \sum_{\forall r \in \mathcal{R}} h_{kn} b_r^{i*} \hat{a}_{nr} e_{nr},$$

where h_{kn} denotes the n th element of vector \mathbf{h}_k . It reveals that, the objective function \hat{f} is separable in each optimization variable e_{nr} . Therefore, \hat{f} can be maximized separately and individually w.r.t. each e_{nr} for $n \in \mathcal{N}, r \in \mathcal{R}$. Consider a summand $h_{kn} b_r^{i*} \hat{a}_{nr} e_{nr}$ of g . Define $\bar{x} + j\tilde{x} \triangleq h_{kn} b_r^{i*} \hat{a}_{nr}$, and $\alpha + j\beta \triangleq e_{nr}$. Substituting these new definitions, the part of function \hat{f} that comprises the variable e_{nr} can be expressed as

$$\tilde{f}(\alpha, \beta) = \underbrace{(\tilde{x} - \bar{x} \tan \theta)}_{\kappa} \alpha + \underbrace{(\bar{x} + \tilde{x} \tan \theta)}_{\tau} \beta.$$

The constraints on phase error values, given by $|e_{nr}| = 1$ and $|\angle e_{nr}| \leq \delta$, can be equivalently expressed as $\alpha^2 + \beta^2 = 1$ and $\alpha \geq \cos \delta$. Substituting $\beta = \pm \sqrt{1 - \alpha^2}$ in the above equation, we get a new equivalent function $f(\alpha) = \kappa\alpha \pm \tau\sqrt{1 - \alpha^2}$. This function comprises the following two variants:

$$f_1(\alpha) = \kappa\alpha + \tau\sqrt{1 - \alpha^2}.$$

$$f_2(\alpha) = \kappa\alpha - \tau\sqrt{1 - \alpha^2}.$$

Note that $\sqrt{1 - \alpha^2}$ is a concave function (square-root function is a non-decreasing concave function and $(1 - \alpha^2)$ is a concave function) [39]. We can identify two cases based on the value of τ . In the first case when $\tau \geq 0$, f_1 is a concave function, f_2 is a convex function, and $f_1 \geq f_2$ for $|\alpha| \leq 1$. Moreover, an optimal point α^* that maximizes f_1 also maximizes \tilde{f} together with $\beta^* = \sqrt{1 - \alpha^{*2}}$. Similarly we argue that, in the second case when $\tau \leq 0$, an optimal point α^* that maximizes the (then) concave function f_2 also maximizes \tilde{f} together with $\beta^* = -\sqrt{1 - \alpha^{*2}}$.

If $\tau \geq 0$, we can obtain the optimal point α^* that maximizes f_1 , by differentiating f_1 w.r.t. α and equating to zero, i.e.,

$$\frac{df_1}{d\alpha} = \kappa - \frac{\tau\alpha}{\sqrt{1 - \alpha^2}} = 0 \implies \alpha^* = \frac{\kappa}{\sqrt{\kappa^2 + \tau^2}}.$$

Similarly, if $\tau \leq 0$ we can obtain the optimal point α^* that maximizes f_2 as

$$\frac{df_2}{d\alpha} = \kappa + \frac{\tau\alpha}{\sqrt{1 - \alpha^2}} = 0 \implies \alpha^* = \frac{\kappa}{\sqrt{\kappa^2 + \tau^2}}.$$

(In the above derivations, we have explicitly used the prior knowledge of sign of τ and used the intermediate result that reveal the sign of α should be same as the sign of κ).

Remember the function f_1 is concave in α if $\tau \geq 0$ and f_2 is concave in α if $\tau \leq 0$. Therefore, if the obtained optimal point α^* is smaller than $\cos \delta$ then we can simply enforce $\alpha^* = \cos \delta$ to get the optimal point within the domain of the phase error that maximizes \tilde{f} . Substituting the expressions for κ and τ we get $e_{nr}^* = \alpha^* + j\beta^*$, where,

$$\begin{aligned} \alpha^* &= \max \left(\cos \delta, \frac{\tilde{\chi} \cos \theta - \bar{\chi} \sin \theta}{|\bar{\chi} + j\tilde{\chi}|} \right), \\ \beta^* &= \text{sign}(\tau) \sqrt{1 - \alpha^{*2}} = \frac{\bar{\chi} + \tilde{\chi} \tan \theta}{|\bar{\chi} + \tilde{\chi} \tan \theta|} \sqrt{1 - \alpha^{*2}}. \end{aligned}$$

Let $\mathbf{Z} \triangleq \left(\mathbf{h}_k (\mathbf{b}^{i*})^T \right) \odot \hat{\mathbf{A}}$. Then, the worst-case error values for all PSs at the BS can be obtained efficiently by computing the error matrix $\mathbf{E}_k^+ = \mathbf{U}^+ + j\mathbf{W}^+$, where,

$$\begin{aligned} u_{nr}^+ &= \max \left(\cos \delta, \frac{\text{Im}(z_{nr}) \cos \theta - \text{Re}(z_{nr}) \sin \theta}{|z_{nr}|} \right), \\ w_{nr}^+ &= \frac{\text{Re}(z_{nr}) + \text{Im}(z_{nr}) \tan \theta}{|\text{Re}(z_{nr}) + \text{Im}(z_{nr}) \tan \theta|} \sqrt{1 - (u_{nr}^+)^2}. \end{aligned}$$

Similarly, we can derive the expression for $\mathbf{E}_k^- = \mathbf{U}^- + j\mathbf{W}^-$, where,

$$\begin{aligned} u_{nr}^- &= \max \left(\cos \delta, \frac{-\text{Im}(z_{nr}) \cos \theta - \text{Re}(z_{nr}) \sin \theta}{|z_{nr}|} \right), \\ w_{nr}^- &= \frac{-\text{Re}(z_{nr}) + \text{Im}(z_{nr}) \tan \theta}{|-\text{Re}(z_{nr}) + \text{Im}(z_{nr}) \tan \theta|} \sqrt{1 - (u_{nr}^-)^2}. \end{aligned}$$

APPENDIX B CONVERGENCE PROPERTIES OF ALG. 1

Lemma 1: *The problems (5) and (6) have unique global optimal solutions.*

Proof: The AP matrix $\hat{\mathbf{A}}$ in problem (5) is a full column rank matrix. In case $\hat{\mathbf{A}}$ is not a full column rank matrix, it can be easily converted into a full column rank matrix without altering the effective HP $\hat{\mathbf{A}}\mathbf{b}$ as follows: Let $\hat{\mathbf{A}} \triangleq [\hat{\mathbf{a}}_1, \dots, \hat{\mathbf{a}}_R] \in \mathbb{C}^{N \times R}$, and a vector $\mathbf{b} \triangleq [b_1, \dots, b_R]^T$ where $N \geq R$. W.l.o.g. let the rank of $\hat{\mathbf{A}}$ be $R-1$, with $\hat{\mathbf{a}}_R$ being linearly dependent on other APs in the matrix $\hat{\mathbf{A}}$, i.e., $\hat{\mathbf{a}}_R = w_1 \hat{\mathbf{a}}_1 + \dots + w_{R-1} \hat{\mathbf{a}}_{R-1}$, where w_1, \dots, w_{R-1} are scalars. Then we have,

$$\begin{aligned} \hat{\mathbf{A}}\mathbf{b} &= b_1 \hat{\mathbf{a}}_1 + \dots + b_R \hat{\mathbf{a}}_R \\ &= b_1 \hat{\mathbf{a}}_1 + \dots + b_R (w_1 \hat{\mathbf{a}}_1 + \dots + w_{R-1} \hat{\mathbf{a}}_{R-1}) \\ &= (b_1 + b_R w_1) \hat{\mathbf{a}}_1 + \dots + (b_{R-1} + b_R w_{R-1}) \hat{\mathbf{a}}_{R-1} \\ &= b'_1 \hat{\mathbf{a}}_1 + \dots + b'_{R-1} \hat{\mathbf{a}}_{R-1} \\ &= \hat{\mathbf{A}}'\mathbf{b}' \end{aligned}$$

where $\hat{\mathbf{A}}' \in \mathbb{C}^{N \times (R-1)}$ is a full column rank matrix.

Due to the full rank property of $\hat{\mathbf{A}}$, the matrix $\hat{\mathbf{A}}^H \hat{\mathbf{A}}$ is positive definite, and the quadratic objective function $\|\hat{\mathbf{A}}\mathbf{b}\|^2 = \mathbf{b}^H \hat{\mathbf{A}}^H \hat{\mathbf{A}}\mathbf{b}$ is strictly convex function in \mathbf{b} . Therefore, the problem (5) has a unique global optimal solution [39]. Following the identical reasoning, we can prove that the problem (6) also has a unique global optimal solution in the i th iteration.

Lemma 2: a) *The optimal solution of problem (5) is a feasible solution of problem (6). b) The optimal value P^* of problem (5) is an upper-bound for problem (6).*

Proof: Let \mathbf{b}^* and P^* be the optimal solution and the optimal value of problem (5) respectively. In problem (6), the union of set of error matrices in the i th iteration $\tilde{\mathcal{E}}^i \triangleq \{\mathcal{E}_1^{i+} \cup \mathcal{E}_1^{i-} \cup \dots \cup \mathcal{E}_K^{i+} \cup \mathcal{E}_K^{i-}\} \subset \mathcal{E}$. Therefore, the set of constraints of problem (6) is a subset of the set constraints of problem (5). Hence the optimal solution \mathbf{b}^* of problem (5) is a feasible solution of problem (6). Moreover, the problems (5) and (6) have a same objective function. Therefore the optimal value of problem (5) is an upper bound for problem (6).

1) **Proof of Theorem 1:** Let \mathbf{b}^{I*} and P^{I*} denote the optimal point and optimal value of problem (6) in the I th iteration respectively. We assume that the constraints in (5b) and (5c) are fulfilled at $\mathbf{b} = \mathbf{b}^{I*}$ for the worst-case error matrices \mathbf{E}_k^{I+} and \mathbf{E}_k^{I-} , $\forall k \in \mathcal{K}$ (hence for all matrices in \mathcal{E}), and the algorithm is terminated. Therefore, the optimal point \mathbf{b}^{I*} of problem (6) is a feasible point of problem (5). Due to Lemma 2a the optimal point \mathbf{b}^* of problem (5) is a feasible point of problem (6) in the I th iteration.

The problems (5) and (6) have the same objective function and domain. Now, for the purpose of contradiction let us assume $P^* < P^{I*}$. The point \mathbf{b}^* is a feasible point of problem (6), which yields a value P^* . This contradicts our assumption that P^{I*} is the optimal value of problem (6). If we assume $P^* > P^{I*}$ we get a similar contradicting result. Therefore we conclude that $P^* = P^{I*}$. Moreover, due to Lemma 1 we get $\mathbf{b}^{I*} = \mathbf{b}^*$. This proves Theorem 1.

2) **Proof of Theorem 2:** Here we follow a similar line of arguments as in [33] to prove Theorem 2. If Alg. 1 terminates after a finite number of I iterations, then $\mathbf{b}^{I*} = \mathbf{b}^*$ according to Theorem 1, which confirms Theorem 2 in this case. On the other hand, if Alg. 1 does not terminate after a finite number of iterations we want to prove that $\lim_{i \rightarrow \infty} f(\mathbf{b}^{i*}) = P^*$. Let $\mathcal{B} \triangleq \{\mathbf{b}^{1*}, \mathbf{b}^{2*}, \dots\}$ be the infinite sequence of optimal points of problem (6). Since the problems (5) and (6) are feasible, the elements of \mathcal{B} are bounded. Due to the practical power budget constraints we can argue w.l.o.g. that the elements of \mathcal{B} are

confined to a compact set. Therefore the sequence \mathcal{B} has limit points [33, 49]. Let $\hat{\mathbf{b}}$ be a limit point. Let $\hat{\mathcal{E}}_k^+$ be a set of error matrices that are associated with the constraint (6b) at point $\mathbf{b} = \hat{\mathbf{b}}$. For the purpose of contradiction assume $f(\hat{\mathbf{b}}) < P^*$, i.e., $\hat{\mathbf{b}}$ is not a feasible point of problem (5). W.l.o.g. let $\bar{\mathbf{E}}_k^+$ be a worst case error matrix of the k th user that violates the constraint (5b) at point $\mathbf{b} = \hat{\mathbf{b}}$. Define the function associated with the constraint (5b) as

$$\hat{f}(\mathbf{b}, \mathbf{E}) \triangleq \text{Im} \left(\mathbf{h}_k^T (\hat{\mathbf{A}} \odot \mathbf{E}) \mathbf{b} \right) - \left(\text{Re} \left(\mathbf{h}_k^T (\hat{\mathbf{A}} \odot \mathbf{E}) \mathbf{b} \right) - \gamma_k \right) \tan \theta.$$

Therefore, we have $\hat{f}(\hat{\mathbf{b}}, \bar{\mathbf{E}}_k^+) > 0$. Moreover, we have $\hat{f}(\hat{\mathbf{b}}, \mathbf{E}) \leq 0, \forall \mathbf{E} \in \hat{\mathcal{E}}_k^+$. Consider a point $\mathbf{b}^{i*} \in \mathcal{B}$ with a worst-case error matrix \mathbf{E}_k^{i+} , and a subsequence $\mathbf{b}^{i*} \rightarrow \hat{\mathbf{b}}$ in \mathcal{B} . Since \mathcal{E} is a compact set, we have a corresponding subsequence of worst-case error matrices $\mathbf{E}_k^{i+} \rightarrow \hat{\mathbf{E}}$ in set $\hat{\mathcal{E}}_k^+$ [33, 49]. By definition of \mathbf{E}_k^{i+} we have $\hat{f}(\mathbf{b}^{i*}, \bar{\mathbf{E}}_k^+) \leq \hat{f}(\mathbf{b}^{i*}, \mathbf{E}_k^{i+})$. Letting $i \rightarrow \infty$ we get $\hat{f}(\hat{\mathbf{b}}, \bar{\mathbf{E}}_k^+) \leq \hat{f}(\hat{\mathbf{b}}, \hat{\mathbf{E}})$. It results in a contradicting result $0 < \hat{f}(\hat{\mathbf{b}}, \bar{\mathbf{E}}_k^+) \leq \hat{f}(\hat{\mathbf{b}}, \hat{\mathbf{E}}) \leq 0$. Hence $f(\hat{\mathbf{b}}) < P^*$ is not possible. Moreover, due to Lemma 2b we have $\lim_{i \rightarrow \infty} f(\mathbf{b}^{i*}) = P^*$.

APPENDIX C

EMPIRICAL RELATION BETWEEN SNR, TNR, AND SER

Fig. 9 plots the empirical relation between SNR, TNR, and SER. For obtaining the relation between SER and SNR in the SNR/SINR fulfillment-based precoding system, Rayleigh-fading-based complex channels with zero mean and unit-variance are assumed. The unit-norm transmit symbols are drawn from the corresponding constellation set. The i.i.d. complex Gaussian noise with zero mean and an appropriate variance are added to the received signal. The channel inversion and projection methods are employed to estimate the transmit symbols [50]. To obtain the relation between SER and TNR in a CI-based precoding system, the received signals are randomly generated on the threshold-margin (set to 1) of all symbols and i.i.d. complex Gaussian noise with zero mean and an appropriate variance are added to them.

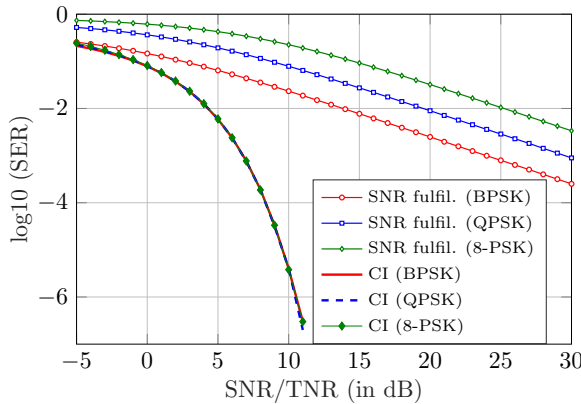


Fig. 9: Empirical relation between SNR, TNR, and SER.

APPENDIX D EMPIRICAL RELATION BETWEEN δ , TNR, AND SER

TABLE IV: SER achieved by the CI-based non-robust precoding for a range of phase error bound δ and TNR for $N = 128$, $R = K = 4$, and QPSK modulation.

δ (deg)	TNR = 2.0	TNR = 2.5	TNR = 3.0
0	4.665 x10 ⁻³	4.120 x10 ⁻⁴	2.320 x10 ⁻⁵
1	4.667 x10 ⁻³	4.126 x10 ⁻⁴	2.333 x10 ⁻⁵
2	4.680 x10 ⁻³	4.138 x10 ⁻⁴	2.340 x10 ⁻⁵
3	4.700 x10 ⁻³	4.148 x10 ⁻⁴	2.351 x10 ⁻⁵
4	4.739 x10 ⁻³	4.185 x10 ⁻⁴	2.355 x10 ⁻⁵
5	4.755 x10 ⁻³	4.208 x10 ⁻⁴	2.370 x10 ⁻⁵
6	4.776 x10 ⁻³	4.248 x10 ⁻⁴	2.400 x10 ⁻⁵
7	4.847 x10 ⁻³	4.290 x10 ⁻⁴	2.460 x10 ⁻⁵
8	4.848 x10 ⁻³	4.373 x10 ⁻⁴	2.490 x10 ⁻⁵
9	4.929 x10 ⁻³	4.431 x10 ⁻⁴	2.533 x10 ⁻⁵
10	4.970 x10 ⁻³	4.555 x10 ⁻⁴	2.600 x10 ⁻⁵

ACKNOWLEDGMENT

The authors would like to thank Minh Trinh Hoang for valuable discussions related to the convergence proof of the algorithm.

REFERENCES

- [1] J. Hoydis, S. ten Brink, and M. Debbah, “Massive MIMO in the UL/DL of cellular networks: How many antennas do we need?” *IEEE J. Select. Areas Commun.*, vol. 31, no. 2, pp. 160–171, Feb. 2013.
- [2] L. Lu, G. Y. Li, A. L. Swindlehurst, A. Ashikhmin, and R. Zhang, “An overview of massive MIMO: Benefits and challenges,” *IEEE J. Select. Topics in Signal Process.*, vol. 8, no. 5, pp. 742–758, Oct. 2014.
- [3] J. Mietzner *et al.*, “Multiple-antenna techniques for wireless communications - A comprehensive literature survey,” *IEEE Commun. Surveys Tutorials*, vol. 11, no. 2, pp. 87–105, Feb. 2009.
- [4] M. Bengtsson and B. Ottersten, “Optimal and suboptimal transmit beamforming,” *Handbook of Antennas in Wireless Commun.*, Aug. 2001.
- [5] C. H. Doan, S. Emami, D. A. Sobel, A. M. Niknejad, and R. W. Brodersen, “Design considerations for 60 GHz CMOS radios,” *IEEE Commun. Mag.*, vol. 42, no. 12, pp. 132–140, Dec. 2004.
- [6] L. Liang, W. Xu, and X. Dong, “Low-complexity hybrid precoding in massive multiuser MIMO systems,” *IEEE Wireless Commun. Letters*, vol. 3, no. 6, pp. 653–656, Dec. 2014.
- [7] F. Sohrabi and W. Yu, “Hybrid digital and analog beamforming design for large-scale antenna arrays,” *IEEE J. Select. Topics in Signal Process.*, vol. 10, no. 3, pp. 501–513, Apr. 2016.
- [8] X. Zhang, A. F. Molisch, and S. Y. Kung, “Variable-phase-shift-based RF-baseband codesign for MIMO antenna selection,” *IEEE Trans. Signal Process.*, vol. 53, no. 11, pp. 4091–4103, Nov. 2005.
- [9] Z. Li *et al.*, “Joint optimization of hybrid beamforming for multi-user massive MIMO downlink,” *IEEE Trans. Wireless Commun.*, vol. 17, no. 6, pp. 3600–3614, Jun. 2018.
- [10] A. F. Molisch *et al.*, “Hybrid beamforming for massive MIMO: A survey,” *IEEE Commun. Mag.*, vol. 55, no. 9, pp. 134–141, Sep. 2017.
- [11] G. Hegde, Y. Cheng, and M. Pesavento, “Hybrid beamforming for large-scale MIMO systems using uplink-downlink duality,” in *Proc. IEEE Int. Conf. on Acoustics, Speech and Signal Process. (ICASSP)*, New Orleans, USA, Mar. 2017.

- [12] F. Sohrabi and W. Yu, "Hybrid analog and digital beamforming for mmWave OFDM large-scale antenna arrays," *IEEE J. Select. Areas Commun.*, vol. 35, no. 7, pp. 1432–1443, Jul. 2017.
- [13] C. Masouros and G. Zheng, "Exploiting known interference as green signal power for downlink beamforming optimization," *IEEE Trans. Signal Process.*, vol. 63, no. 14, pp. 3628–3640, Jul. 2015.
- [14] C. Masouros *et al.*, "Known interference in the cellular downlink: A performance limiting factor or a source of green signal power?" *IEEE Commun. Mag.*, vol. 51, no. 10, pp. 162–171, Oct. 2013.
- [15] G. Zheng *et al.*, "Rethinking the role of interference in wireless networks," *IEEE Commun. Mag.*, vol. 52, no. 11, pp. 152–158, Nov. 2014.
- [16] S. Timotheou, G. Zheng, C. Masouros, and I. Krikidis, "Exploiting constructive interference for simultaneous wireless information and power transfer in multiuser downlink systems," *IEEE J. Select. Areas Commun.*, vol. 34, no. 5, pp. 1772–1784, May 2016.
- [17] M. Schubert and H. Boche, "Solution of the multiuser downlink beamforming problem with individual SINR constraints," *IEEE Trans. Veh. Technol.*, vol. 53, no. 1, pp. 18–28, Jan. 2004.
- [18] G. Hegde, C. Masouros, and M. Pesavento, "Analog beamformer design for interference exploitation based hybrid beamforming," in *Proc. IEEE Sensor Array and Multichannel Signal Process. Workshop (SAM)*, Sheffield, UK, Jul. 2018.
- [19] R. Vannithamby and S. Talwar, *Towards 5G: Applications, Requirements & Candidate Technologies*. John Wiley & Sons Incorporated, 2017.
- [20] S. Wu, L. Chiu, K. Lin, and T. Chang, "Robust hybrid beamforming with phased antenna arrays for downlink SDMA in indoor 60 GHz channels," *IEEE Trans. Wireless Commun.*, vol. 12, no. 9, pp. 4542–4557, Sep. 2013.
- [21] M. R. A. Khandaker, C. Masouros, and K. K. Wong, "Constructive interference based secure precoding: A new dimension in physical layer security," *IEEE Trans. on Inform. Forensics and Security*, vol. 13, no. 9, pp. 2256–2268, Sep. 2018.
- [22] D. P. Bertsekas, *Nonlinear programming*, 2nd ed. Athena scientific Belmont, 1999.
- [23] P. V. Amadori and C. Masouros, "Large scale antenna selection and precoding for interference exploitation," *IEEE Trans. Commun.*, vol. 65, no. 10, pp. 4529–4542, Oct. 2017.
- [24] A. Li and C. Masouros, "Exploiting constructive mutual coupling in P2P MIMO by analog-digital phase alignment," *IEEE Trans. Wireless Commun.*, vol. 16, no. 3, pp. 1948–1962, Mar. 2017.
- [25] Y. Yu *et al.*, "A 60 GHz phase shifter integrated with LNA and PA in 65 nm CMOS for phased array systems," *IEEE Journal of Solid-State Circuits*, vol. 45, no. 9, pp. 1697–1709, Sep. 2010.
- [26] W. T. Li *et al.*, "60-GHz 5-bit phase shifter with integrated VGA phase-error compensation," *IEEE Trans. on Microwave Theory and Techniques*, vol. 61, no. 3, pp. 1224–1235, Mar. 2013.
- [27] S. Gimenez *et al.*, "Performance evaluation of analog beamforming with hardware impairments for mmW massive MIMO communication in an urban scenario," *Sensors*, vol. 16, no. 10, p. 1555, 2016.
- [28] F. Rusek *et al.*, "Scaling up MIMO: Opportunities and challenges with very large arrays," *IEEE Signal Process. Mag.*, vol. 30, no. 1, pp. 40–60, Jan. 2013.
- [29] H. Yin, D. Gesbert, M. Filippou, and Y. Liu, "A coordinated approach to channel estimation in large-scale multiple-antenna systems," *IEEE J. Select. Areas Commun.*, vol. 31, no. 2, pp. 264–273, Feb. 2013.
- [30] R. O. Duda, P. E. Hart, and D. G. Stork, *Pattern Classification*. New York, USA: Wiley-Interscience, 2000.
- [31] C. Masouros and E. Alsusa, "Dynamic linear precoding for the exploitation of known interference in MIMO broadcast systems," *IEEE Trans. Wireless Commun.*, vol. 8, no. 3, pp. 1396–1404, Mar. 2009.
- [32] F. G. Vázquez, J.-J. Rückmann, O. Stein, and G. Still, "Generalized semi-infinite programming: A tutorial," *Journal of Computational and Applied Mathematics*, vol. 217, no. 2, pp. 394 – 419, 2008.
- [33] S. A. Gustafson and K. O. Kortanek, "Numerical treatment of a class of semi-infinite programming problems," *Naval Research Logistics Quarterly*, vol. 20, no. 3, pp. 477–504, 1973.
- [34] S. Y. Wu, S. C. Fang, and C. J. Lin, "Relaxed cutting plane method for solving linear semi-infinite programming problems," *Journal of Optimization Theory and Applications*, vol. 99, no. 3, pp. 759–779, 1998.
- [35] E. Karipidis, N. D. Sidiropoulos, and Z. Q. Luo, "Quality of service and Max-Min fair transmit beamforming to multiple cochannel multicast groups," *IEEE Trans. Signal Process.*, vol. 56, no. 3, pp. 1268–1279, Mar. 2008.
- [36] K. C. Toh, M. J. Todd, and R. H. Tütüncü, "SDPT3 — A Matlab software package for semidefinite programming, version 1.3," *Optimization Methods and Software*, vol. 11, no. 1-4, pp. 545–581, 1999.
- [37] Y. Yang and M. Pesavento, "A unified successive pseudoconvex approximation framework," *IEEE Trans. Signal Process.*, vol. 65, no. 13, pp. 3313–3328, Jul. 2017.
- [38] G. Hegde, Y. Yang, C. Steffens, and M. Pesavento, "Parallel low-complexity M-PSK detector for large-scale MIMO systems," in *Proc. IEEE Sensor Array and Multichannel Signal Process. Workshop (SAM)*, Rio de Janeiro, Brazil, Jul. 2016, pp. 1–5.
- [39] S. Boyd and L. Vandenberghe, *Convex Optimization*. New York, NY, USA: Cambridge University Press, 2004.
- [40] D. P. Palomar and M. Chiang, "A tutorial on decomposition methods for network utility maximization," *IEEE J. Select. Areas Commun.*, vol. 24, no. 8, pp. 1439–1451, Aug. 2006.
- [41] A. Alkhateeb, G. Leus, and R. W. Heath, "Limited feedback hybrid precoding for multi-user millimeter wave systems," *IEEE Trans. Wireless Commun.*, vol. 14, no. 11, pp. 6481–6494, Nov. 2015.
- [42] G. Hegde and M. Pesavento, "Joint user selection and hybrid analog-digital beamforming in massive MIMO systems," in *Proc. IEEE Sensor Array and Multichannel Signal Process. Workshop (SAM)*, Sheffield, UK, Jul. 2018.
- [43] D. Bansal, A. Kumar, A. Sharma, P. Kumar, and K. J. Rangra, "Design of novel compact anti-stiction and low insertion loss RF MEMS switch," *Microsystem Technologies*, vol. 20, no. 2, pp. 337–340, Feb. 2014.
- [44] E. Elhamifar and R. Vidal, "Block-sparse recovery via convex optimization," *IEEE Trans. Signal Process.*, vol. 60, no. 8, pp. 4094–4107, Aug. 2012.
- [45] C. Steffens and M. Pesavento, "Block- and rank-sparse recovery for direction finding in partly calibrated arrays," *IEEE Trans. Signal Process.*, vol. 66, no. 2, pp. 384–399, Jan. 2018.
- [46] O. E. Ayach, S. Rajagopal, S. Abu-Surra, Z. Pi, and R. W. Heath, "Spatially sparse precoding in millimeter wave MIMO systems," *IEEE Trans. Wireless Commun.*, vol. 13, no. 3, pp. 1499–1513, Mar. 2014.
- [47] J. Wang and D. P. Palomar, "Worst-case robust MIMO transmission with imperfect channel knowledge," *IEEE Trans. Signal Process.*, vol. 57, no. 8, pp. 3086–3100, Aug. 2009.
- [48] A. Pascual-Iserte, D. P. Palomar, A. I. Perez-Neira, and M. A. Lagunas, "A robust maximin approach for MIMO communications with imperfect channel state information based on convex optimization," *IEEE Trans. Signal Process.*, vol. 54, no. 1, pp. 346–360, Jan. 2006.
- [49] S. Wu, D. Li, L. Qi, and G. Zhou, "An iterative method for solving KKT system of the semi-infinite programming," *Optimization Methods and Software*, vol. 20, no. 6, pp. 629–643, 2005.
- [50] D. Tse and P. Viswanath, *Fundamentals of Wireless Communication*. Cambridge University Press, 2005.